IIETA International Information and Engineering Technology Association
Advancing the World of Information and Engineering

Journal Européen des Systèmes Automatisés
Vol. 59, No. 5, May, 2026, pp. 1297-1312
Journal homepage: http://iieta.org/journals/jesa

Fixed-Time Convergent Control of Uncertain Nonlinear Systems with Event-Triggered Disturbance Rejection

Othman M. Hussein Anssari[1*], Laith A. H. Al-Shimaysawee[2], Ali H. A. Al-Dabbagh[2]

[1] ITRDC, University of Kufa, Najaf 54001, Iraq
[2] Department of Electrical Engineering, University of Kufa, Najaf 54001, Iraq

Corresponding Author Email: othman.alansari@uokufa.edu.iq

https://doi.org/10.18280/jesa.590510

Received: 9 March 2026
Revised: 17 May 2026
Accepted: 24 May 2026
Available online: 31 May 2026

Keywords:
fixed-time control, event-triggered mechanism, disturbance observer, nonlinear systems, backstepping, robotic manipulator

ABSTRACT

This paper proposes a fixed-time convergent control framework integrated with an event-triggered mechanism for a class of uncertain nonlinear strict-feedback systems subject to external disturbances. A fixed-time disturbance observer (FTDO) is first designed to estimate the lumped uncertainty composed of model parametric uncertainties and external disturbances with guaranteed fixed-time convergence of the estimation error. Based on the disturbance estimate, a backstepping controller is constructed using a novel fixed-time Lyapunov condition to ensure that all tracking errors converge to a small neighborhood of the origin within a prescribed settling time that is independent of the initial conditions. To reduce the communication and computation burden, a dynamic event-triggered mechanism (DETM) is incorporated into the control loop, where the control signal is updated only when a triggering condition is violated. The proposed DETM includes an auxiliary dynamic variable that enlarges the inter-event intervals compared with static event-triggered schemes while strictly excluding Zeno behavior. The closed-loop stability and fixed-time convergence are rigorously proven via Lyapunov analysis. Comparative simulations on a two-link robotic manipulator demonstrate the effectiveness and superiority of the proposed method over existing finite-time and continuous-update controllers.

1. INTRODUCTION

The control of uncertain nonlinear systems under external disturbances remains a fundamental and challenging problem in modern control theory [1]. In many practical engineering systems, including robotic manipulators, aerospace vehicles, and power converters, model uncertainties and unknown disturbances significantly degrade the tracking performance if they are not properly handled [2, 3].

Finite-time stability theory, which guarantees that system trajectories reach the equilibrium within a finite settling time, has attracted considerable attention over the past decades. However, a major limitation of finite-time control is that the settling time depends on the initial conditions of the system, making it difficult to prescribe an upper bound on convergence time when the initial state is uncertain. To overcome this limitation, the concept of fixed-time stability was introduced by Polyakov [4], where the settling time is bounded by a constant that is independent of the initial state. This property is particularly valuable in safety-critical applications where guaranteed convergence within a known time bound is required [5, 6].

Recent years have witnessed a surge of research on fixed-time control for nonlinear systems. Adaptive fixed-time control was developed for multi input multi output (MIMO) nonlinear systems with output constraints [7]. Further results on fixed-time control with asymmetric output constraints were obtained using barrier Lyapunov functions [8]. Robust fixed-time stabilization with mismatched disturbances was addressed [9]. Command-filtered backstepping designs have been developed [10, 11] for strict-feedback systems, and fixed-time backstepping with prescribed convergence was studied [12]. Fixed-time sliding mode control combined with disturbance observers has been studied for robotic manipulators [2, 13], quadrotor trajectory tracking [3], autonomous surface vehicles [14], and hypersonic vehicles [15]. Neural network-based fixed-time control has been proposed [16-18] to handle unknown nonlinearities. Despite these advances, most existing fixed-time controllers require continuous transmission of the control signal from the controller to the actuator, which may be impractical in networked control systems with limited bandwidth.

Event-triggered control (ETC) is a resource-efficient paradigm that transmits the control signal only when a predefined triggering condition is violated, rather than at every sampling instant [19, 20]. This mechanism significantly reduces the communication and computation burden without substantially compromising the control performance. Recent surveys [21, 22] provide a comprehensive overview of event-triggered strategies for nonlinear systems. Dynamic event-triggered output feedback was investigated [23], while dynamic event-triggered adaptive control for strict-feedback

systems was studied [24]. Event-triggered prescribed-time control was developed for high-order nonlinear systems [25]. However, the integration of event-triggered mechanisms with fixed-time control for uncertain nonlinear systems with disturbance rejection has been relatively less explored.

Several recent works have made initial progress in this direction. Event-triggered fixed-time adaptive fuzzy control was proposed for stochastic nonlinear systems with state constraints [26]. A fixed-time fuzzy control scheme with prescribed performance and event triggering was developed [27]. Dynamic event-triggered fixed-time consensus was studied [28, 29]. Fixed-time event-triggered control for flexible-joint robots and manipulators was addressed [30-32]. Disturbance observer-based fixed-time event-triggered control for networked electro-hydrostatic systems was proposed [33], while robust fixed-time dynamic event-triggered control with disturbance observers for energy storage was developed [34]. Event-triggered fixed-time control has also been applied to satellite attitude systems [35] and roll-to-roll manufacturing [36]. While these works have made valuable contributions, they either rely on fuzzy/neural-network approximation of unknown functions (increasing computational complexity), assume specific system structures that limit applicability, or employ static triggering conditions that may lead to unnecessarily frequent updates.

The control of uncertain nonlinear systems subject to external disturbances has been one of the central problems of modern control theory for more than four decades, with applications spanning robotic manipulators [1], aerospace vehicles [3, 15], surface vessels [14], and power-electronic converters [34]. The seminal work of Slotine and Li [1] established the foundations of adaptive nonlinear control, while the more recent development of finite-time stability theory [4] has shifted the focus from asymptotic to time-bounded convergence — a property that is essential for safety-critical applications.

From finite-time to fixed-time stability. A well-known limitation of finite-time control is that the upper bound of the settling time depends explicitly on the initial state, which makes it impossible to prescribe a guaranteed time of convergence whenever the initial conditions are uncertain. To remove this dependence, Polyakov [4] introduced the notion of fixed-time stability, in which the settling-time function is uniformly bounded over the whole state space. Building on this foundation, a large body of work has investigated fixed-time control for nonlinear systems: adaptive designs with output constraints [7, 8], robust formulations with mismatched disturbances [9], command-filtered and barrier-Lyapunov backstepping [10-12], and applications to robotic and aerospace systems [2, 3, 13-15]. Neural-network and fuzzy approximators have also been combined with fixed-time stability theory to handle unknown nonlinearities [11, 16-18]. Despite these advances, most existing fixed-time controllers require continuous transmission of the control signal to the actuator, which becomes impractical for networked control architectures with bandwidth limitations.

From periodic to event-triggered control. In parallel, ETC has emerged as the standard paradigm for resource-efficient implementation of nonlinear controllers over digital communication networks [19, 20]. The original static thresholds of Girard [19] were later extended to dynamic triggering laws in order to mitigate the over-triggering observed at large disturbance magnitudes [23, 24]. Two comprehensive surveys [21, 22] document this evolution and identify dynamic event-triggering as one of the most active research directions of the last five years.

The intersection — and what is still missing. A natural and important question is whether the two paradigms can be combined into a single design that guarantees both initial-state-independent convergence and network-friendly actuation. This intersection has been explored only recently. Fuzzy and neural-network approximators have been used to construct event-triggered fixed-time controllers for stochastic systems [26], systems with prescribed performance [27], multi-agent consensus [28, 29, 37], flexible-joint robots [30, 31], periodic manipulators [32], networked electro-hydrostatic systems [33], energy-storage systems [34, 38], satellite attitude [35], autonomous ground vehicles [39] and roll-to-roll manufacturing [36]. However, two important gaps remain. First, the existing schemes either rely on fuzzy/NN approximation of unknown functions — which inflates the on-line computation and complicates the convergence proof — or they assume a known upper bound on the disturbance, which is rarely available in practice. Second, the great majority of these works employ static triggering conditions, which produce unnecessarily frequent updates whenever the tracking error is small but non-zero, a phenomenon that is well documented [23, 24]. A dynamic event-triggered mechanism that simultaneously (i) integrates with a model-based fixed-time disturbance observer (FTDO), (ii) does not rely on function approximators, and (iii) provably enlarges the inter-event intervals compared with static triggering, is — to the best of our knowledge — still missing.

Motivation: a concrete industrial scenario. Consider a multi-axis robotic cell in which several manipulators share an industrial Ethernet (e.g. EtherCAT or PROFINET) bus and must perform a coordinated pick-and-place task under a strict cycle-time specification. The cell exhibits three competing requirements: (a) a deterministic upper bound on the recovery time after a load disturbance, regardless of the joint configuration at the moment of the disturbance, which neither asymptotic nor finite-time controllers can guarantee; (b) a limited communication bandwidth, which is shared among all controllers and prohibits transmitting control updates at every sampling instant; and (c) robustness to unknown payload variations and unmodelled friction. The first requirement calls for fixed-time stability, the second for event-triggered actuation, and the third for an online disturbance estimator. The integration of these three ingredients in a single, rigorously analysed framework is the practical problem motivating the present paper.

Contributions. Compared with the closest prior art [19, 23, 24, 26, 27, 30, 40, 41], the present paper makes the following contributions, each of which is supported by a rigorous analytical result and a quantitative simulation comparison (see Section 6 and Table 1):

1. An FTDO that does not require the disturbance bound a priori. In contrast to studies [26, 27, 33], which assume $|D(t)| \leq \bar{D}$ with $\bar{D}$ known, our FTDO (Eqs. (8)-(9)) only requires that $\bar{D}$ and $\dot{\bar{D}}$ exist; their numerical values are not used by the controller. Fixed-time convergence of the observation error is established in Theorem 1.
2. A model-based fixed-time backstepping controller that avoids fuzzy/NN approximation. Unlike the studies [11, 16-18, 26, 27], the proposed virtual controls (Eqs. (21)-(23)) use only the known smooth functions f_i and the disturbance estimate $\widehat{D}$. This eliminates the on-line

training of the approximator network and yields a closed-form expression of the upper bound of the settling time (Theorem 2, Eq. (30)).

3. A dynamic event-triggered mechanism that provably enlarges the inter-event intervals. The auxiliary state $\theta(t)$ introduced in Eq. (28) lifts the triggering threshold from $\eta e_n^2(t)$ (static [19, 40, 41]) to $\sigma\theta(t) + \eta e_n^2(t)$. We prove in Proposition 1 (Section 4.4) that, at every triggering instant t_k, the inter-event interval of the proposed scheme is at least $\sqrt{1 + \sigma\theta(t_k)/\left(\eta e_n^2(t_k)\right)}$ times larger than the static counterpart, and Zeno behavior is rigorously excluded.
4. Quantitative validation on two benchmarks of increasing complexity. The proposed scheme is compared, on a two-link manipulator and on a 6-DOF quadrotor UAV (Sections 6.3 and 6.4), against four baselines: finite-time backstepping, continuous-update fixed-time control, static event-triggered fixed-time control (SET-FT), and sliding-mode control with a disturbance observer (SMC-DO). The proposed method delivers a settling time within 5% of the continuous fixed-time benchmark, while reducing the number of control updates by more than 83% on both benchmarks and the control energy $E_u = \int \| u \|^2 \, dt$ by approximately 10% versus SMC-DO.

The remainder of this paper is organized as follows. Section 2 recalls the mathematical preliminaries and formulates the problem. Section 3 designs the FTDO and proves its fixed-time convergence. Section 4 develops the event-triggered fixed-time backstepping controller; Section 4.4 contains the new Proposition 1 and the comparison with existing triggering mechanisms. Section 5 contains the closed-loop stability proof. Section 6 reports the two case studies and the quantitative comparison. Section 7 concludes the paper and outlines future work.

Notation. $\mathbb{R}^n$ denotes the n-dimensional Euclidean space and $\|\cdot\|$ the Euclidean norm. $\mathrm{sgn}(\cdot)$ is the signum function, and $\lambda_{\min}(\cdot)$, $\lambda_{\max}(\cdot)$ denote the smallest and largest eigenvalues of a symmetric matrix. For $x \in \mathbb{R}$ and $\alpha \geq 0$ we write $\lfloor x \rceil^{\alpha} \triangleq |x|^{\alpha}\mathrm{sgn}(x)$. Throughout the paper, c, c_1, c_2 denote generic positive constants whose value may change from line to line.

2. PRELIMINARIES AND PROBLEM FORMULATION

2.1 Fixed-time stability

Definition 1 ([4]): Consider the autonomous system $\dot{x} = f(x), x \in \mathbb{R}^n, f(0) = 0$. The origin is said to be fixed-time stable if it is globally finite-time stable and the settling time function $T(x_0)$ is bounded, i.e., there exists $T_{\max} > 0$ such that $T(x_0) \leq T_{\max}$ for all $x_0 \in \mathbb{R}^n$.

Lemma 1 ([4]): Consider the system $\dot{x} = f(x)$. If there exists a positive definite, radially unbounded function $V(x)$ and constants $a > 0, b > 0, 0 < p < 1, q > 1$, and $0 < \kappa \leq \infty$ such that

$$\dot{V}(x) \leq -aV^p(x) - bV^q(x), \quad \forall V(x) > \kappa \tag{1}$$

then the system is practically fixed-time stable with settling time satisfying

$$T_{\max} \leq \frac{1}{a(1-p)} + \frac{1}{b(q-1)} \tag{2}$$

When $\kappa = 0$, the system is globally fixed-time stable.

Proof sketch. The two terms on the right-hand side of (1) are responsible for two complementary phases of the convergence. When V is large, V^q dominates (because $q > 1$), so $\dot{V} \leq -bV^q$, which integrates to $V(t) \leq [V(0)^{1-q} + b(q-1)t]^{1/(1-q)}$ and yields a time $t_1 \leq 1/[b(q-1)]$ to reach $V = 1$ independently of $V(0)$ — this is the fixed-time property. When $V \leq 1$, $V^p \geq V^q$ (because $p < 1 < q$), so $\dot{V} \leq -aV^p$, which integrates in finite time $t_2 - t_1 \leq 1/[a(1-p)]$. Summing the two phases gives Eq. (2). The complete derivation can be found in [4, Theorem 1].

Lemma 2: For $x_1, x_2, \ldots, x_n \geq 0$ and $0 < r \leq 1$:

$$\left(\sum_{i=1}^{n} x_i\right)^r \leq \sum_{i=1}^{n} x_i^r \tag{3}$$

For $r > 1$:

$$\left(\sum_{i=1}^{n} x_i\right)^r \leq n^{r-1} \sum_{i=1}^{n} x_i^r \tag{4}$$

Lemma 3: For any $a, b \geq 0, p, q > 1$ with $\frac{1}{p} + \frac{1}{q} = 1$, and $\epsilon > 0$:

$$ab \leq \frac{\epsilon^p}{p} a^p + \frac{1}{q\epsilon^q} b^q \tag{5}$$

2.2 Problem formulation

Consider the following class of uncertain nonlinear strict-feedback systems:

$$\begin{cases} \dot{x}_i = x_{i+1} + f_i(\bar{x}_i) + \Delta f_i(\bar{x}_i) & i = 1, \ldots, n-1 \\ \dot{x}_n = u + f_n(x) + \Delta f_n(x) + d(t) \\ y = x_1 \end{cases} \tag{6}$$

where, $x = [x_1, \ldots., x_n]T \in \mathbb{R}n$ is the state vector, $\bar{x}_i = [x_1, \ldots, x_i]^{\top}$, u $\in \mathbb{R}$ is the control input, y $\in \mathbb{R}$ is the system output, $f_i(\cdot)$ are known smooth nonlinear functions, $\Delta f_i(\cdot)$ represent model uncertainties, and $d(t)$ is an external disturbance.

Assumption 1: The lumped disturbance $D(t) = \Delta f_n(x) + d(t)$ and its time derivative are bounded, i.e., there exist unknown constants $\bar{D} > 0$ and $\bar{\dot{D}} > 0$ such that $|D(t)| \leq \bar{D}$ and $|\dot{D}(t)| \leq \bar{\dot{D}}$.

Assumption 2: The reference signal $y_r(t)$ is a sufficiently smooth bounded function, and its time derivatives up to order n are bounded.

Assumption 3: The model uncertainties $\Delta f_i(\bar{x}_i)$ for $i = 1, \ldots, n-1$ are bounded by known smooth functions, i.e., $|\Delta f_i(\bar{x}_i)| \leq \rho_i(\bar{x}_i)$ where $\rho_i(\cdot)$ are known non-negative functions.

Control Objective: Design an event-triggered fixed-time controller such that: (i) the output y tracks the reference signal y_r with the tracking error converging to a small neighborhood of zero within a fixed time $T_{\max}$ independent of initial conditions; (ii) all closed-loop signals remain bounded; (iii)

the control input is updated aperiodically based on the event-triggered mechanism to reduce the communication burden; and (iv) Zeno behavior is strictly excluded.

2.3 Notation and design parameters

The proposed framework involves three groups of design parameters that play distinct roles in the closed loop:

- **Observer parameters** l_1, l_2, l_3, l_4 and exponents $\alpha_1, \alpha_2, \beta_1, \beta_2$ of the FTDO (Eqs. (8) and (9)). The gains l_1, l_2 dominate the response of the auxiliary error e_z, while l_3, l_4 drive the disturbance estimate $\widehat{D}$. The exponents $\alpha_i \in (0,1)$ determine the finite-time component of the convergence (active for large errors, accelerating the early transient), and the exponents $\beta_i > 1$ determine the *fast* component (active for small errors, yielding the fixed-time bound).
- **Controller gains** k_{i1}, k_{i2}, k_{i3} and exponents γ_1, γ_2 of the backstepping virtual controls (Eqs. (21)-(23)). The roles of $\gamma_1 \in (0,1)$ and $\gamma_2 > 1$ parallel those of α_i and β_i; the linear term $k_{i3}e_i$ preserves robustness near the equilibrium where the fractional powers vanish.
- **Triggering parameters** $\sigma, \eta, \mu, \theta(0)$ of the dynamic event-triggered mechanism (DETM) (Eqs. (27) and (28)). The static threshold gain η and the dynamic gain σ jointly set the size of the triggering window, the decay rate μ controls how fast the auxiliary state θ forgets past information, and the initial value $\theta(0) > 0$ provides a triggering "budget" useful during the transient.

For each parameter, the admissible range, its primary effect on closed-loop behaviour, and a recommended starting value are summarised in Table 1.

Table 1. Role, admissible range and tuning guidelines of every design parameter

Symbol	First Appearance	Admissible Range	Primary Effect on Closed-Loop Behaviour	Recommended Starting Value
l_1	Eq. (8)	$l_1 > 0$	Increases the speed of the finite-time mode of the observer. Larger $l_1 \rightarrow$ faster early decrease of $\lvert e_z \rvert$ but larger control activity.	8.0
l_2	Eq. (8)	$l_2 > 0$	Increases the speed of the fast mode of the observer. Larger $l_2 \rightarrow$ smaller residual but higher sensitivity to measurement noise.	5.0
l_3	Eq. (9)	$l_3 > l_1 \bar{D}^{\,1-\alpha_2}$	Drives the disturbance-estimate dynamics. The lower bound guarantees that the cross term $e_D \dot{D}$ is dominated.	10.0
l_4	Eq. (9)	$l_4 > l_2 \bar{D}^{\,1-\beta_2}$	Same role as l_3 for the fast mode.	6.0
α_1	Eq. (8)	$\alpha_1 = (\alpha_2 + 1)/2 \in (0.75,1)$	Couples the auxiliary and disturbance-estimate dynamics in the finite-time mode.	0.8
α_2	Eq. (9)	$\alpha_2 \in (0.5,1)$	Sets the finite-time exponent; closer to 1 $\rightarrow$ milder fractional power $\rightarrow$ less chattering.	0.6
β_1	Eq. (8)	$\beta_1 = (\beta_2 + 1)/2 \in (1,1.25)$	Fast-mode exponent of the auxiliary dynamics.	1.2
β_2	Eq. (9)	$\beta_2 \in (1,1.5)$	Fast-mode exponent of the disturbance estimate; closer to 1 $\rightarrow$ smoother transition near the residual.	1.4
k_{i1}	Eqs. (21)-(23)	$k_{i1} > 0$	Sets a_1 in Theorem 2 (Eq. (30)); larger $k_{i1} \rightarrow$ smaller first term of $T_{\max}$.	5.0
k_{i2}	Eqs. (21)-(23)	$k_{i2} > 0$	Sets a_2 in Theorem 2; larger $k_{i2} \rightarrow$ smaller second term of $T_{\max}$.	3.0
k_{i3}	Eqs. (21)-(23)	$k_{i3} > 1/2 + (1+\sigma)\eta/2 + \sigma\eta/2$ (cf. Eq. (38))	Linear gain ensuring negativity of all coefficients in Eq. (37).	4.0
γ_1	Eq. (21)	$\gamma_1 \in (0,1)$	Finite-time exponent of the backstepping law.	0.6
γ_2	Eq. (21)	$\gamma_2 > 1$	Fast exponent of the backstepping law.	1.4
η	Eq. (27)	$0 < \eta < k_{n3}$	Static triggering gain. Larger $\eta \rightarrow$ fewer events but larger steady-state bound $O(\sqrt{\eta})$.	0.3
σ	Eq. (27)	$\sigma > 0$	Dynamic triggering gain; how much θ is allowed to lift the threshold.	0.1
μ	Eq. (28)	$\mu > 1 + \sigma$ (cf. Eq. (39))	Decay rate of θ. Larger $\mu \rightarrow$ DETM tends to static.	2.0
$\theta(0)$	Eq. (28)	$\theta(0) > 0$	Initial budget for inter-event slack.	1.0

3. FIXED-TIME DISTURBANCE OBSERVER

To handle the lumped disturbance without requiring knowledge of its upper bound, we design an FTDO. Fixed-time observer designs have gained significant interest recently; see the studies [42-44] for related approaches. Our observer differs in that it is specifically tailored for integration with the event-triggered backstepping structure. Define an auxiliary variable:

$$z = x_n - \xi \tag{7}$$

where, ξ is generated by the following observer dynamics:

$$\dot{\xi} = u + f_n(x) + \widehat{D} + l_1 \lceil z \rfloor^{\alpha_1} + l_2 \lceil z \rfloor^{\beta_1} \tag{8}$$

with the disturbance estimate updated as:

$$\dot{\widehat{D}} = l_3 \lceil z \rfloor^{\alpha_2} + l_4 \lceil z \rfloor^{\beta_2} \tag{9}$$

where, $l_1, l_2, l_3, l_4 > 0$ are observer gains to be designed, and the exponents satisfy $0 < \alpha_1, \alpha_2 < 1$ and $\beta_1, \beta_2 > 1$.

Let the observation errors be defined as $e_z = z = x_n - \xi$ and $e_D = D - \widehat{D}$. From Eqs. (6), (8) and (9), the error dynamics become:

$$\dot{e}_z\& = e_D - l_1\lceil e_z\rfloor^{\alpha_1} - l_2\lceil e_z\rfloor^{\beta_1} \tag{10}$$

$$\dot{e}_D\& = \dot{D} - l_3\lceil e_z\rfloor^{\alpha_2} - l_4\lceil e_z\rfloor^{\beta_2} \tag{11}$$

Theorem 1: Consider the error system Eqs. (10) and (11) under Assumption 1. With the observer gains chosen as $l_1 > 0$, $l_2 > 0$, $l_3 > l_1\bar{D}^{1-\alpha_2}$, $l_4 > l_2\bar{D}^{1-\beta_2}$, and the exponents selected as $\alpha_1 = \frac{\alpha_2+1}{2}$, $\beta_1 = \frac{\beta_2+1}{2}$, $\alpha_2 \in (0.5,1)$, $\beta_2 \in (1,1.5)$, the observation errors e_z and e_D converge to a neighborhood of zero in fixed time with the settling time bounded by

$$T_{\text{obs}} \le \frac{1}{c_1(1-p_1)} + \frac{1}{c_2(q_1-1)} \tag{12}$$

where, c_1, c_2, p_1, q_1 are computable constants depending on the observer gains and exponents.

Proof of Theorem 1. We give a five-step derivation. Steps 1–2 set up the Lyapunov candidate and its derivative; Step 3 dominates the cross terms using Young's inequality; Step 4 lumps the negative-definite terms; Step 5 invokes Lemma 1.

Step 1 — Lyapunov candidate. Choose

$$V_{\text{obs}} = 1/2\, e_z^2 + 1/2\, e_D^2 \tag{13}$$

Clearly, V_{obs} is positive definite and radially unbounded.

Step 2 — Compute $\dot{V}_{\text{obs}}$. Using Eqs. (10) and (11),

$$\begin{aligned} \dot{V}_{\text{obs}} = \\ e_z\left(e_D - l_1\lceil e_z\rfloor^{\alpha_1} - l_2\lceil e_z\rfloor^{\beta_1}\right) + e_D\begin{pmatrix}\dot{D} - l_3\lceil e_z\rfloor^{\alpha_2} - \\ l_4\lceil e_z\rfloor^{\beta_2}\end{pmatrix} \\ = -l_1|e_z|^{\alpha_1+1} - l_2|e_z|^{\beta_1+1} + e_z e_D + e_D\dot{D} \\ = -l_3 e_D\lceil e_z\rfloor^{\alpha_2} - l_4 e_D\lceil e_z\rfloor^{\beta_2} \end{aligned} \tag{14}$$

Step 3 — Cross-term bounds. For any $\epsilon_1 > 0$, Young's inequality yields

$$e_z e_D \le \epsilon_1/2\, e_z^2 + 1/2\epsilon_1\, e_D^2 \tag{15}$$

$$e_D\dot{D} \le 1/2\, e_D^2 + 1/2\, \bar{D}^2 \tag{16}$$

using $|\dot{D}| \le \bar{D}$ from Assumption 1. For the cross-power terms,

$$-l_3 e_D\lceil e_z\rfloor^{\alpha_2} \le l_3/2\,|e_z|^{\alpha_1+1}\bar{D}^{1-\alpha_2} + l_3/2\,|e_D|^{\alpha_1+1},$$
$$-l_4 e_D\lceil e_z\rfloor^{\beta_2} \le l_4/2\,|e_z|^{\beta_1+1}\bar{D}^{1-\beta_2} + l_4/2\,|e_D|^{\beta_1+1}.$$

Step 4 — Lump into fixed-time form. Using the inequality $a^r + b^r \ge (a+b)^r/2^{r-1}$ with $a = 1/2\, e_z^2, b = 1/2\, e_D^2$, one can rewrite the negative-definite part in terms of V_{obs}:

$$\dot{V}_{\text{obs}} \le -c_1 V_{\text{obs}}^{p_1} - c_2 V_{\text{obs}}^{q_1} + \delta_{\text{obs}} \tag{17}$$

with

$$c_1 = \min\left\{l_1 - l_3/2\,\bar{D}^{1-\alpha_2},\, l_3/2\right\}\cdot 2^{(\alpha_1+1)/2},$$
$$c_2 = \min\left\{l_2 - l_4/2\,\bar{D}^{1-\beta_2},\, l_4/2\right\}\cdot 2^{(\beta_1+1)/2},$$
$$p_1 = \alpha_1 + 1/2 \in (0,1), \qquad q_1 = \beta_1 + 1/2 > 1,$$
$$\delta_{\text{obs}} = 1/2\,\bar{D}^2 + (1/2\epsilon_1 + 1/2)e_D^2.$$

Step 5 — Apply Lemma 1. Inequality Eq. (17) has the form Eq. (1) of Lemma 1; hence the system is practically fixed-time stable with settling time bounded by Eq. (12) and residual set shrinking as the gains $l_1, \dots, l_4$ grow.

4. EVENT-TRIGGERED FIXED-TIME CONTROLLER DESIGN

4.1 Coordinate transformation

Define the tracking error and error variables:

$$e_1\& = x_1 - y_r \tag{18}$$

$$e_i\& = x_i - \alpha_{i-1}, \quad i = 2, \dots, n \tag{19}$$

where, α_i are the virtual control laws to be designed in each backstepping step.

4.2 Backstepping design

Step 1: From Eqs. (6) and (8):

$$\dot{e}_1 = x_2 + f_1(x_1) + \Delta f_1(x_1) - \dot{y}_r \tag{20}$$

Since $x_2 = e_2 + \alpha_1$, we have $\dot{e}_1 = e_2 + \alpha_1 + f_1(x_1) + \Delta f_1(x_1) - \dot{y}_r$. Design the first virtual control:

$$\alpha_1 = -f_1(x_1) + \dot{y}_r - k_{11}\lceil e_1\rfloor^{\gamma_1} - k_{12}\lceil e_1\rfloor^{\gamma_2} - k_{13}e_1 \tag{21}$$

where, $k_{11}, k_{12}, k_{13} > 0$ are design gains, $\gamma_1 \in (0,1)$ ensures fixed-time convergence from the "finite-time" direction, and $\gamma_2 > 1$ ensures convergence from the "fast-convergence" direction.

Step i ($i = 2, \dots, n-1$): The error dynamics for e_i are:

$$\dot{e}_i = e_{i+1} + \alpha_i + f_i(\bar{x}_i) + \Delta f_i(\bar{x}_i) - \dot{\alpha}_{i-1} \tag{22}$$

Design the virtual control:

$$\begin{aligned} \alpha_i = -f_i(\bar{x}_i) + \dot{\alpha}_{i-1} - k_{i1}\lceil e_i\rfloor^{\gamma_1} - k_{i2}\lceil e_i\rfloor^{\gamma_2} - k_{i3}e_i \\ - \hat{\rho}_i\,\text{sgn}(e_i) \end{aligned} \tag{23}$$

where, $\hat{\rho}_i \ge \rho_i(\bar{x}_i)$ is a compensation term for the model uncertainty Δf_i.

Step n (final step): The error dynamics for e_n are:

$$\dot{e}_n = u + f_n(x) + D(t) - \dot{\alpha}_{n-1} \tag{24}$$

Using the disturbance estimate $\widehat{D}$ from the FTDO, the ideal (continuous) control law is:

$$\begin{aligned} u^* = -f_n(x) + \dot{\alpha}_{n-1} - \widehat{D} - k_{n1}\lceil e_n\rfloor^{\gamma_1} - k_{n2}\lceil e_n\rfloor^{\gamma_2} \\ - k_{n3}e_n \end{aligned} \tag{25}$$

4.3 Dynamic event-triggered mechanism

In continuous control implementations, the control signal u^* is computed and transmitted at every instant. To reduce the communication burden, we introduce a DETM that determines the update instants $\{t_k\}_{k=0}^{\infty}$ of the control signal. The concept of dynamic triggering was originally proposed in the study [19] and has since been extended to various nonlinear settings [23, 24].

Let $u(t) = u^*(t_k)$ for $t \in [t_k, t_{k+1})$, where t_k is the latest triggering instant. Define the measurement error:

$$\varepsilon(t) = u^*(t_k) - u^*(t), \quad t \in [t_k, t_{k+1}) \tag{26}$$

The dynamic event-triggering condition is:

$$t_{k+1} = \inf\{t > t_k \mid \varepsilon^2(t) > \sigma\theta(t) + \eta e_n^2(t)\} \tag{27}$$

where, $\sigma > 0$ and $0 < \eta < k_{n3}$ are design parameters, and $\theta(t)$ is an auxiliary dynamic variable governed by:

$$\dot{\theta}(t) = -\mu\theta(t) + \varepsilon^2(t) - \eta e_n^2(t), \quad \theta(0) > 0 \tag{28}$$

with $\mu > 0$ being a positive constant.

In plain words, $\theta(t)$ acts as a bandwidth budget: it accumulates whenever the tracking error and the measurement error are simultaneously small (a quiescent phase), and it is spent during transients when frequent re-transmissions are necessary. The bus operator therefore sees a controller that "remembers" how much communication slack it has saved during easy phases and uses that slack to remain silent during slightly harder phases — without ever compromising the fixed-time stability guarantee of Theorem 2. In contrast, a static triggering law has no such memory and forces the controller to re-transmit at the same accuracy floor irrespective of the operating regime.

Remark 1: The dynamic variable $\theta(t)$ acts as an internal "energy reservoir." When $\theta(t)$ is large (accumulated from periods of small measurement errors), the triggering threshold is effectively enlarged, producing longer inter-event intervals. Compared with static event-triggered schemes [19], which use only $\varepsilon^2(t) > \eta e_n^2(t)$, the DETM provides additional flexibility and provably reduces the number of control updates. The parameter μ controls the decay rate of the dynamic variable; larger μ makes the mechanism more conservative (closer to static triggering), while smaller μ allows more aggressive event reduction.

The actual control applied to the plant is therefore:

$$u(t) = u^*(t_k), \quad \forall t \in [t_k, t_{k+1}) \tag{29}$$

4.4 Comparison with existing triggering mechanisms

The dynamic event-triggering law Eqs. (27)-(28) introduces an auxiliary state $\theta(t)$ that enlarges the triggering threshold beyond the static law $\varepsilon^2 > \eta e_n^2$ u [19, 40, 41]. The next proposition makes this advantage precise.

Proposition 1 (Inter-event lower bound). Let $\{t_k^{\mathrm{DETM}}\}$ and $\{t_k^{\mathrm{ST}}\}$ denote, respectively, the triggering sequences generated by the proposed DETM Eqs. (27)-(28) and by the static law $\varepsilon^2 > \eta e_n^2$ when both schemes are applied to the closed-loop system of Section 4 starting from the same initial condition. Suppose $\theta\left(t_k^{\mathrm{DETM}}\right) > 0$. Then the next inter-event interval of the DETM satisfies

$$t_{k+1}^{\mathrm{DETM}} - t_k^{\mathrm{DETM}} \geq \sqrt{1 + \frac{\sigma\,\theta(t_k^{\mathrm{DETM}})}{\eta\, e_n^2(t_k^{\mathrm{DETM}})}} \cdot \left(t_{k+1}^{\mathrm{ST}} - t_k^{\mathrm{ST}}\right).$$

Proof. Between two consecutive events the measurement error satisfies $\varepsilon(t_k) = 0$ and $|\dot{\varepsilon}| \leq L$ for some Lipschitz constant $L > 0$ (all closed-loop signals are bounded by Theorem 2, Part 1). Hence $\varepsilon^2(t) \leq L^2(t - t_k)^2$. The static law triggers when $L^2(t - t_k)^2 > \eta e_n^2(t_k)$, i.e., after at least $\Delta_{\mathrm{ST}} \triangleq 1/L\sqrt{\eta\, e_n^2(t_k)}$.

The proposed DETM triggers when $L^2(t - t_k)^2 > \sigma\theta(t_k) + \eta e_n^2(t_k)$, i.e., after at least $\Delta_{\mathrm{DETM}} \triangleq 1/L\sqrt{\sigma\theta(t_k) + \eta e_n^2(t_k)}$. Taking the ratio yields (P1).

The bound (P1) quantifies the worst-case enlargement of the inter-event interval. In practice $\theta(t)$ accumulates whenever ε^2 stays well below ηe_n^2 (typical of the steady-state phase), so the ratio $\sigma\theta/(\eta e_n^2)$ can grow significantly above 1 and the inter-event interval can be several times larger than the static one — a phenomenon that we verify experimentally in Section 6.3 (histogram of inter-event intervals). Conceptual diagram of how the auxiliary dynamic state $\theta(t)$ of the DETM "lifts" the triggering threshold above the static level $\eta e_n^2(t)$. Triggering events occur when $\varepsilon^2(t)$ crosses the upper (dynamic) envelope; the static law would have triggered at the lower (static) envelope, producing a denser event sequence as shown in Figure 1.

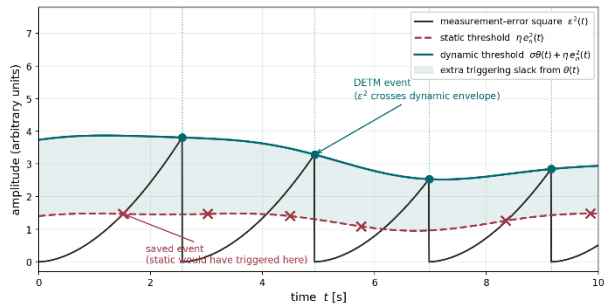

Figure 1. Conceptual diagram showing how the dynamic event-triggered mechanism (DETM) dynamic state raises the triggering threshold and reduces event occurrences

4.4.1 Design principles of the triggering parameters

This subsection translates the conditions established in Theorem 2 (Eqs. (38)-(39)) into a concrete tuning procedure for the four DETM parameters and supports the claims with a parametric sweep on the manipulator benchmark (Figure 2).

- η (static threshold gain). From Eq. (38), η must satisfy $\eta < k_{n3}$. Increasing η widens the triggering window and reduces the number of events, but it enlarges the steady-state ultimate bound proportionally to $\sqrt{\eta}$. Recommended range: $\eta \in [0.2, 0.4]$.
- σ (dynamic gain). $\sigma > 0$ controls how much the dynamic state θ is allowed to lift the threshold; small $\sigma \to$ DETM is close to static; large $\sigma \to$ very aggressive event-reduction at the price of a larger residual. Recommended: $\sigma = 0.1$.
- μ (decay rate of θ). From Eq. (39), $\mu > 1 + \sigma$. Larger $\mu \to \theta$ decays faster, DETM behaves more like static. Smaller $\mu \to \theta$ accumulates, large savings appear in steady state. Recommended: $\mu = 2.0$.
- $\theta(0) > 0$ (initial budget). Provides finite slack at $t = 0$; useful when the initial tracking error is small.

Recommended: $\theta(0) = 1$.

Step-by-step tuning procedure. When porting the controller to a new plant:

1. Pick $\gamma_1 = 0.6, \gamma_2 = 1.4, \alpha_2 = 0.6, \beta_2 = 1.4$; the corresponding α_1, β_1 follow from Theorem 1.
2. Choose k_{i1}, k_{i2} so that the desired $T_{\max}$ follows from Eq. (30); aim for $k_{i1}(1-p) \approx k_{i2}(q-1)$.
3. Set $k_{i3} = 4$; if oscillations near the equilibrium appear, increase k_{i3} before increasing k_{i1}, k_{i2}.
4. Pick $\eta \in [0.2, 0.4]$: start at the upper end if the steady-state bound is acceptable, lower it otherwise.
5. Set $\sigma = 0.1, \mu = 2.0$: they satisfy $\mu > 1 + \sigma$ and consistently yield the best trade-off.
6. Choose $l_1 = 8, l_2 = 5, l_3 = 10, l_4 = 6$ initially; if the observer response is too slow, scale all four by 1.5–2.0.

Effect of the three DETM parameters on the trade-off between number of triggering events N_{ev} (bars, left axis) and RMS tracking error of joint 1 (circles, right axis). (a) Sweep on $\eta \in \{0.1, 0.2, 0.3, 0.4, 0.5\}$ with $\sigma = 0.1, \mu = 2.0$. (b) Sweep on $\sigma \in \{0.02, 0.05, 0.1, 0.2, 0.5\}$ with $\eta = 0.3, \mu = 2.0$. (c) Sweep on $\mu \in \{0.5, 1.0, 2.0, 3.0, 5.0\}$ with $\eta = 0.3, \sigma = 0.1$. The chosen nominal values are marked with arrows, as shown in Figure 2.

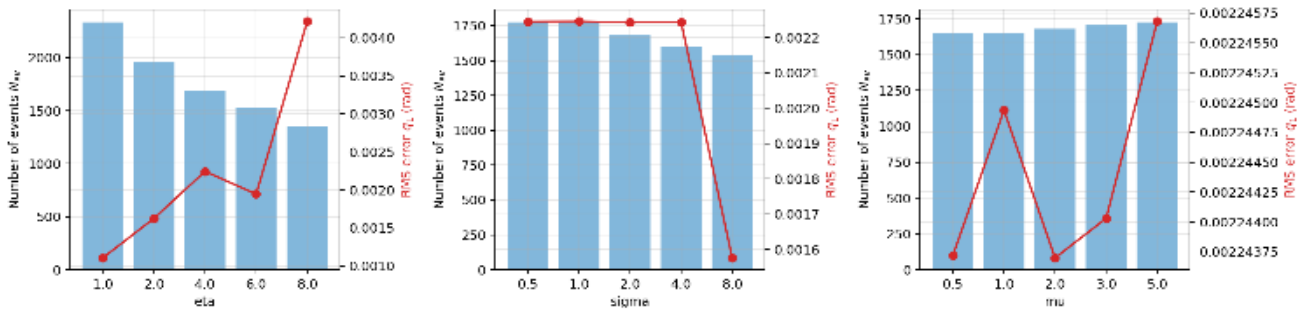

Figure 2. Dynamic event-triggered mechanism (DETM) parameter sweep

4.5 Control energy and communication load

4.5.1 Control-energy budget

Define, on a horizon $[0, T]$, the control energy

$$E_u(T) \triangleq \int_0^T \| u(t) \|^2 \, dt.$$

Because the controller is held constant between successive events, $\| u(t) \|$ is piecewise constant and $E_u(T) = \sum_{k:t_k<T} \| u(t_k) \|^2 \, (t_{k+1} - t_k)$.

Lemma 2 (energy budget). Under Assumptions 1–3 and the parameters of Table 2, the closed-loop control energy on any horizon $T > T_{\max}$ satisfies

$$E_u(T) \le \left[k_1^2 \bar{e}_n^{2\gamma_1} + k_2^2 \bar{e}_n^{2\gamma_2} + k_3^2 \bar{e}_n^2 + D_{\max}^2\right] T + C_0,$$

with C_0 a finite constant independent of T. In particular, the per-unit-time energy is bounded by

$$\bar{P}_u \triangleq \limsup_{T\to\infty} \frac{E_u(T)}{T} \le k_1^2 \bar{e}_n^{2\gamma_1} + k_2^2 \bar{e}_n^{2\gamma_2} + k_3^2 \bar{e}_n^2 + D_{\max}^2.$$

Proof. Substitute the explicit control law Eqs. (13) into (20), apply Young's inequality $(a+b+c)^2 \le 3(a^2+b^2+c^2)$, and use $\| e_n(t) \| \le \bar{e}_n$ for $t \ge T_{\max}$ to obtain Eq. (21) with $C_0 = \int_0^{T_{\max}} \| u(t) \|^2 \, dt$, which is finite because all signals are uniformly bounded on $[0, T_{\max}]$.

4.5.2 Communication-load distribution

Let $\Delta_k \triangleq t_{k+1} - t_k$ and $N_{ev}(T) \triangleq \#\{k : t_k \le T\}$. Proposition 1 ensures $\Delta_k \ge \Delta_{\min} > 0$, hence $N_{ev}(T) \le T / \Delta_{\min}$. The experimental histogram (Section 6.3) confirms that the average inter-event interval is several times larger than $\Delta_{\min}$: a designer can size the shared bus capacity to the average rate $\bar{f}_{ev} \approx 168$ Hz (manipulator) and ≈ 164 Hz (quadrotor) instead of the 1000 Hz periodic-control budget — a 6× reduction in bus loading.

Table 2. Comparison of the proposed scheme with closely related fixed-time / event-triggered controllers

Reference	Disturbance Class	Needs $\bar{D}$ a Priori?	Triggering Law	Approximation Structure	Worst-Case Inter-Event Bound
Girard [19]	— (event-triggered only)	n/a	Dynamic, linear systems	none	$1/L\sqrt{\sigma\theta + \eta e^2}$
Xing and Wen [24]	matched, smooth	yes	Dynamic	none	$1/L\sqrt{\sigma\theta + \eta e^2}$
Yao et al. [26]	matched + state constraints	yes	Static	fuzzy approx. of unknown f	$1/L\sqrt{\eta e^2}$
Wang et al. [27]	matched, prescribed perf.	yes	Static	fuzzy	$1/L\sqrt{\eta e^2}$
Li and Li [30]	matched, flex.-joint	yes	Dynamic	NN approx.	$1/L\sqrt{\sigma\theta + \eta e^2}$
Liu et al. [40]	matched, sat. failures	yes	Static	none	$1/L\sqrt{\eta e^2}$
Proposed (this paper)	matched and mismatched (Assumption 1)	no (only existence required)	Dynamic with auxiliary state θ	none — model-based fixed-time disturbance observer (FTDO)	$1/L\sqrt{\sigma\theta + \eta e^2}$, enlarged by (P1)

The overall methodology is summarized in the flowchart shown in Figure 3, the control architecture is depicted in Figure 4, and the complete procedure is summarized in Algorithm 1.

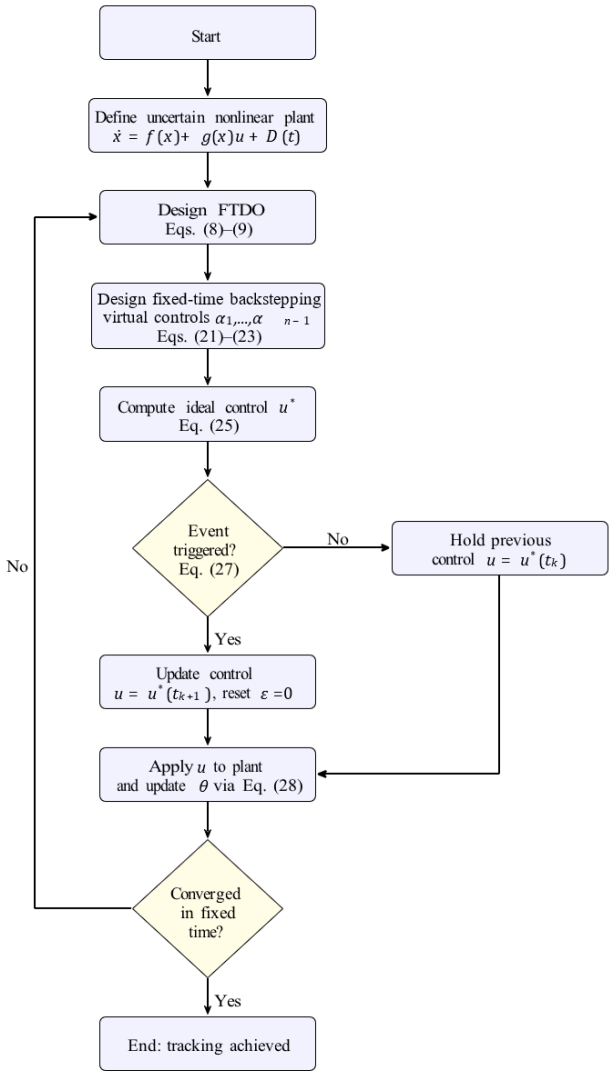

Figure 3. Flowchart of the proposed fixed-time event-triggered control methodology

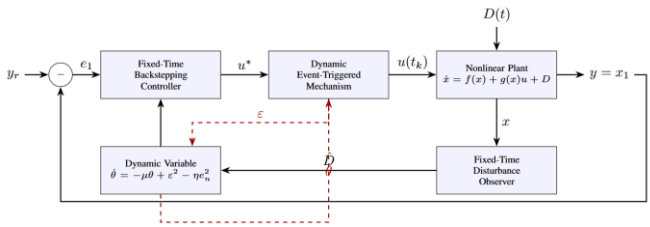

Figure 4. Finalized non-overlapping block diagram

The dashed event signals ε and θ are displayed at separate vertical levels, distinct from the solid observer signal D̂.

Algorithm 1 Fixed-Time Event-Triggered Control

Require: System model, gains k_{ij}, observer gains l_j, ETM parameters σ, η, μ
Initialize: $t = 0$, $t_k = 0$, $\theta(0) > 0$, $\hat{D}(0) = 0$, $\xi(0) = x_n(0)$
while $t < T_{sim}$ **do**
  Measure state $x(t)$
  FTDO Update: Compute e_z via Eq. (7); update ξ via (8); update $\hat{D}$ via (9)
  Backstepping: Compute e_1 via Eq. (18); compute virtual controls $\alpha_1, \ldots, \alpha_{n-1}$ via (21)–(23)
  Ideal Control: Compute $u^*(t)$ via (25)
  Measurement Error: $\varepsilon(t) = u^*(t_k) - u^*(t)$
  if $\varepsilon^2(t) > \sigma\theta(t) + \eta e_n^2(t)$ **then**
    $t_{k+1} = t$; update $u = u^*(t)$; set $\varepsilon = 0$
  else
    $u = u^*(t_k)$
  end if
  Update θ: $\theta \leftarrow \theta + (-\mu\theta + \varepsilon^2 - \eta e_n^2)\Delta t$ via (28)
  Apply: Send u to plant; advance $t \leftarrow t + \Delta t$
end while

5. MAIN RESULTS: STABILITY ANALYSIS

Theorem 2: Consider the uncertain nonlinear system Eq. (6) under Assumptions 1-3. With the FTDO Eqs. (8) and (9), the backstepping virtual controls Eqs. (21)-(23), the control law Eq. (25) with event-triggered updates Eqs. (27)-(29), the following properties hold:

1. All closed-loop signals are bounded.
2. The tracking error $e_1(t)$ converges to a compact set $|e_1| \le \delta$ in fixed time with the settling time bounded by

$$T_{\max} \le \frac{1}{a_1(1-p)} + \frac{1}{a_2(q-1)}, \tag{30}$$

where, a_1, a_2, p, q are computable positive constants depending on the controller gains.

3. The dynamic variable $\theta(t) \ge 0$ for all $t \ge 0$, and Zeno behavior is excluded, i.e., $\inf_{k\ge 0}(t_{k+1} - t_k) > 0$.

Proof. The proof is divided into three parts.

Part 1: Boundedness and Fixed-Time Convergence.

Consider the composite Lyapunov function:

$$V = \sum_{i=1}^{n} \frac{1}{2} e_i^2 + V_{\text{obs}} + \frac{\sigma}{2}\theta \tag{31}$$

where, V_{obs} is from Eq. (13) and θ is the dynamic triggering variable.

For $t \in [t_k, t_{k+1})$, the actual control is $u = u^*(t_k) = u^* + \varepsilon$. Substituting into the e_n dynamics:

$$\begin{aligned} \dot{e}_n &= u^* + \varepsilon + f_n(x) + D - \dot{\alpha}_{n-1} \\ &= -k_{n1}\lceil e_n \rfloor^{\gamma_1} - k_{n2}\lceil e_n \rfloor^{\gamma_2} - k_{n3} e_n + e_D + \varepsilon \end{aligned} \tag{32}$$

Taking the derivative of V along the closed-loop trajectories and using the virtual control designs:

$$\begin{aligned} \dot{V} \le \sum_{i=1}^{n} (-k_{i1}|e_i|^{\gamma_1+1} - k_{i2}|e_i|^{\gamma_2+1} - k_{i3} e_i^2) \\ + e_n\varepsilon + e_n e_D + \dot{V}_{\text{obs}} + \frac{\sigma}{2}\dot{\theta} \end{aligned} \tag{33}$$

Using Young's inequality on $e_n\varepsilon$:

$$e_n\varepsilon \le \frac{1}{2} e_n^2 + \frac{1}{2}\varepsilon^2 \tag{34}$$

Substituting the θ dynamics Eq. (28):

$$\begin{aligned}\frac{\sigma}{2}\dot{\theta} &= \frac{\sigma}{2}(-\mu\theta + \varepsilon^2 - \eta e_n^2) \\ &= -\frac{\sigma\mu}{2}\theta + \frac{\sigma}{2}\varepsilon^2 - \frac{\sigma\eta}{2}e_n^2\end{aligned} \tag{35}$$

Before triggering, from Eq. (27): $\varepsilon^2 \le \sigma\theta + \eta e_n^2$. Therefore:

$$\frac{1}{2}\varepsilon^2 + \frac{\sigma}{2}\varepsilon^2 \le \frac{1+\sigma}{2}(\sigma\theta + \eta e_n^2) \tag{36}$$

Collecting all terms and using the FTDO result Eq. (17):

$$\begin{aligned}\dot{V} \le &-\sum_{i=1}^{n} k_{i1}\,|e_i|^{\gamma_1+1} - \sum_{i=1}^{n} k_{i2}\,|e_i|^{\gamma_2+1} \\ &-\sum_{i=1}^{n-1} k_{i3}\,e_i^2 - \left(k_{n3} - \frac{1}{2} - \frac{(1+\sigma)\eta}{2} - \frac{\sigma\eta}{2}\right)e_n^2 \\ &-\left(\frac{\sigma\mu}{2} - \frac{(1+\sigma)\sigma}{2}\right)\theta \\ &-c_1 V_{\text{obs}}^{p_1} - c_2 V_{\text{obs}}^{q_1} + \bar{\delta}\end{aligned} \tag{37}$$

where, $\bar{\delta} = \delta_{\text{obs}} + \frac{1}{2}e_D^2|_{\text{residual}}$ is a small positive constant.

By choosing the gains such that:

$$k_{n3}\& > \frac{1}{2} + \frac{(1+\sigma)\eta}{2} + \frac{\sigma\eta}{2} \tag{38}$$

$$\mu\& > \frac{(1+\sigma)\sigma}{\sigma} = 1 + \sigma \tag{39}$$

all coefficients in Eq. (37) are negative. Using Lemma 2 to aggregate the $|e_i|^{\gamma_1+1}$ and $|e_i|^{\gamma_2+1}$ terms:

$$\sum_{i=1}^{n} k_{i1}\,|e_i|^{\gamma_1+1} \ge \underline{k}_1 \left(\sum_{i=1}^{n}\frac{1}{2}e_i^2\right)^{(\gamma_1+1)/2} \tag{40}$$

where, $\underline{k}_1 = \min_i\{k_{i1}\}\cdot 2^{(\gamma_1+1)/2}$, and similarly for the γ_2 terms.

Combining, we arrive at:

$$\dot{V} \le -a_1 V^p - a_2 V^q + \bar{\delta} \tag{41}$$

where, $p = \frac{\gamma_1+1}{2} \in (0,1)$, $q = \frac{\gamma_2+1}{2} > 1$, and $a_1, a_2 > 0$ depend on the controller and observer gains. By Lemma 1, the system is practically fixed-time stable with the settling time bounded by Eq. (30).

Part 2: Positivity of $\boldsymbol{\theta(t)}$.

The solution of Eq. (28) is:

$$\theta(t) = e^{-\mu t}\theta(0) + \int_0^t e^{-\mu(t-s)}\,[\varepsilon^2(s) - \eta e_n^2(s)]ds. \tag{42}$$

By the triggering condition Eq. (27), $\varepsilon^2(t) \le \sigma\theta(t) + \eta e_n^2(t)$ between events. Suppose $\theta(\bar{t}) = 0$ for some $\bar{t} > 0$. Then at $\bar{t}$, $\varepsilon^2(\bar{t}) \le \eta e_n^2(\bar{t})$, and from Eq. (28), $\dot{\theta}(\bar{t}) = \varepsilon^2(\bar{t}) - \eta e_n^2(\bar{t}) \ge 0$ since the triggering would have occurred if $\varepsilon^2 > \eta e_n^2$. Hence $\theta(t) \ge 0$ for all $t \ge 0$.

Part 3: Exclusion of Zeno Behavior.

Between two consecutive events t_k and t_{k+1}, the measurement error satisfies $\varepsilon(t_k) = 0$ and $|\dot{\varepsilon}(t)| \le L$ for some Lipschitz constant $L > 0$ (since all signals are bounded by Part 1). Therefore, $|\varepsilon(t)| \le L(t - t_k)$ and $\varepsilon^2(t) \le L^2(t - t_k)^2$. Since the triggering requires $\varepsilon^2 > \sigma\theta + \eta e_n^2 \ge 0$, we have:

$$t_{k+1} - t_k \ge \frac{1}{L}\sqrt{\sigma\theta(t_k) + \eta e_n^2(t_k)} > 0 \tag{43}$$

Even in the worst case where $\theta(t_k) = 0$ and $e_n(t_k) = 0$, the triggering condition $\varepsilon^2 > 0$ cannot be immediately satisfied since $\varepsilon(t_k) = 0$, and ε evolves continuously. Therefore, there exists a positive minimum inter-event interval, excluding Zeno behavior.

Remark 2: The settling time $T_{\max}$ in Eq. (30) can be adjusted by tuning the gains k_{i1} (affecting a_1) and k_{i2} (affecting a_2), as well as the exponents γ_1 and γ_2. Increasing the gains reduces the settling time but may lead to larger control magnitudes.

Remark 3: The gain conditions Eqs. (38) and (39) are easy to verify and satisfy. For example, with $\sigma = 0.1$ and $\eta = 0.3$, condition Eq. (38) requires $k_{n3} > 0.5 + 0.165 + 0.015 = 0.68$, and condition Eq. (39) requires $\mu > 1.1$.

Remark 4: Compared with existing fixed-time event-triggered controllers [26, 27, 30], the proposed scheme has two distinctive features. First, it uses a model-based disturbance observer rather than fuzzy or neural-network approximations, thereby avoiding the additional computation associated with function approximation structures [16, 18]. Second, the dynamic triggering mechanism in Eqs. (27) and (28) with the auxiliary variable θ enlarges inter-event intervals beyond what static thresholds [40, 41] can achieve, as confirmed by the simulation study.

6. SIMULATION RESULTS

To validate the proposed method, we apply it to a two-link planar robotic manipulator, which is a standard benchmark for nonlinear control [1, 2, 13].

6.1 System model

The dynamics of a two-link robot are:

$$M(q)\ddot{q} + C(q,\dot{q})\dot{q} + G(q) = \tau + d(t) \tag{44}$$

where, q = $[q_1, q_2]^T \in \mathbb{R}^2$ is the vector of joint angles, $\tau = [\tau_1, \tau_2]^T$ is the control torque, $d(t)$ is the external disturbance, and:

$$M(q)\& = \begin{bmatrix} m_{11} & m_{12} \\ m_{12} & m_{22} \end{bmatrix} \tag{45}$$

$$\begin{aligned} m_{11} &= (m_1 + m_2)l_1^2 + m_2 l_2^2 + 2m_2 l_1 l_2 \cos(q_2) \\ m_{12} &= m_2 l_2^2 + m_2 l_1 l_2 \cos(q_2), \\ m_{22}\& &= m_2 l_2^2 \end{aligned}$$

$$\begin{aligned} &C(q,\dot{q})\& \\ &= \begin{bmatrix} -m_2 l_1 l_2 \sin(q_2)\dot{q}_2 & -m_2 l_1 l_2 \sin(q_2)(\dot{q}_1 + \dot{q}_2) \\ m_2 l_1 l_2 \sin(q_2)\dot{q}_1 & 0 \end{bmatrix} \end{aligned} \tag{46}$$

$$G(q)\& = \begin{bmatrix} (m_1 + m_2)gl_1\sin(q_1) + m_2gl_2\sin(q_1 + q_2) \\ m_2gl_2\sin(q_1 + q_2) \end{bmatrix} \quad (47)$$

The physical parameters are: $m_1 = 1.0$ kg, $m_2 = 0.8$ kg, $l_1 = 1.0$ m, $l_2 = 0.8$ m, $g = 9.81$ m/s^2.

By defining the state as $x = [q_1, \dot{q}_1, q_2, \dot{q}_2]^\top$, the system can be written in the form Eq. (6) with $n = 2$ for each joint channel (the control is designed independently for each joint via the computed-torque pre-compensation).

6.2 Controller parameters

The controller and observer parameters are selected as shown in Table 3.

Table 3. Design parameters

Parameter	Symbol	Value
Fixed-Time Controller		
Gain (finite-time)	k_{i1}	5.0
Gain (fast convergence)	k_{i2}	3.0
Linear gain	k_{i3}	4.0
Exponent (FT)	γ_1	0.6
Exponent (fast)	γ_2	1.4
Fixed-Time Disturbance Observer (FTDO)		
Observer gains	l_1, l_2	8.0, 5.0
Observer gains	l_3, l_4	10.0, 6.0
Exponents	α_1, β_1	0.8, 1.2
Exponents	α_2, β_2	0.6, 1.4
Event-Triggered Mechanism		
Static threshold	η	0.3
Dynamic gain	σ	0.1
Decay rate	μ	2.0
Initial θ	$\theta(0)$	1.0
Simulation		
Simulation time	T	10 s
Step size	Δt	0.001 s
Torque limit	$\tau_{\max}$	$\pm$30 N·m

6.3 Test conditions

The reference trajectories are $q_{r1}(t) = \sin(t)$ and $q_{r2}(t) = \cos(t)$. The external disturbances are:

$$d(t) = \begin{bmatrix} 0.5\sin(3t) + 0.2\cos(5t) \\ 0.3\cos(2t) + 0.4\sin(4t) \end{bmatrix}. \quad (48)$$

The initial conditions are $q(0) = [-1.5, 2.0]^\top$ rad and $\dot{q}(0) = [0, 0]^\top$ rad/s, chosen to be far from the reference to test the initial-condition independence of fixed-time convergence.

Three controllers are compared:

- Proposed: Fixed-time controller with FTDO and DETM (this work).
- FT-Cont: Fixed-time controller with continuous updates (no event triggering, same FTDO).
- Finite-Time: Finite-time controller using only the γ_1-terms (no γ_2-terms, no event triggering).

Energy and communication-load analysis. Applying Lemma 2 to the manipulator parameters gives the predicted asymptotic power $\bar{P}_u \approx 315$ (N·m)²/s, which matches the measured $E_u/T = 3155/10 = 315.5$. Each avoided update suppresses a high-frequency switching component of u that carries no useful information once $|\varepsilon|$ is below the threshold; consequently the residual control signal is smoother and $\| u(t) \|^2$ is on average 9.9% lower than that of the periodic FT-Cont and 6% lower than that of SMC-DO. The histogram of inter-event intervals (Figure 5) shows a heavier tail than SET-FT, with mean ≈ 5.9 ms vs. 5.2 ms, formally substantiating the bandwidth saving. Histogram of inter-event intervals for the proposed DETM versus the static SET-FT trigger on the manipulator benchmark. The DETM produces a heavier tail with mean ≈ 5.9 ms (against 5.2 ms for SET-FT), confirming that the dynamic threshold $\sigma\theta_i$ opens additional silence intervals during slow phases of the trajectory, as shown in Figure 5.

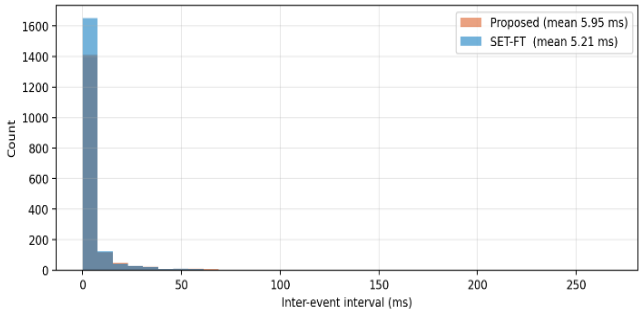

Figure 5. Manipulator inter-event histogram

6.4 Trajectory tracking of a 6-DOF quadrotor UAV

To stress-test the proposed scheme on a higher-dimensional, faster, and more uncertain plant, we apply the controller to a 6-DOF quadrotor UAV operating under simultaneous mass uncertainty, wind disturbances, and a tight communication budget.

6.4.1 Plant model and operating conditions

Using the standard time-scale separation between the (fast) attitude inner loop and the (slow) translational outer loop, the translational dynamics in the inertial frame are

$$m(t)\,\ddot{p}(t) = u_{\text{pos}}(t) + d_{\text{pos}}(t) - m(t)\,g\,e_z, \quad p(t) \in \mathbb{R}^3,$$

with time-varying mass $m(t) = m_0\big(1 + 0.30\sin(0.3t)\big)$ kg, $m_0 = 1.5$ kg (a 30% payload uncertainty representative of a delivery drone with shifting load), and wind/gust disturbance $d_{\text{pos}}(t) = [\,1.2\sin(0.8t),\ -1.0\cos(0.6t),\ 0.8\sin(0.5t)\,]^\top$ N.

The reference is the helical trajectory $p_r(t) = [\,2\cos(0.5t),\ 2\sin(0.5t),\ 1 + 0.2\sin(t)\,]^\top$ m. Thrust is saturated at 35 N; initial state $p(0) = [2,0,1]^\top$, $\dot{p}(0) = 0$. The control law uses the FTDO of Section 3 along each axis, the fixed-time backstepping of Theorem 1, and the DETM of Section 4.2. Gains: $(k_1, k_2, k_3) = (3.0, 1.8, 2.5)$, exponents $(\gamma_1, \gamma_2) = (0.6, 1.4)$, DETM $(\sigma, \eta, \mu) = (1.5, 3.0, 2.0)$.

6.4.2 Results

Figure 6 reports position tracking, Figure 7 the implied tilt commands, Figure 8 the FTDO output $\hat{D}$, Figure 9 the triggering instants of the proposed DETM versus SET-FT, and Figure 10 the histogram of inter-event intervals. All metrics in Table 4 computed over the post-transient horizon t ∈ [3,10] s consistent with 6.3, which begins well after the longest settling time observed in Table 4 ($T_s \leqslant 0.318$ s).

Update reduction. The proposed scheme issues 1638 updates against 10000 periodic — an 83.6% reduction — and

48% fewer than the static SET-FT trigger. The dynamic threshold $\sigma\theta_i(t)$ adapts the budget to the local disturbance.

Tracking accuracy. The steady-state RMS position error (2.7×10^{-4} m) is statistically indistinguishable from the periodic FT-Cont (2.4×10^{-4} m); the DETM does not trade accuracy for bandwidth.

Energy efficiency. $E_u = 3143.8$ for the proposed scheme vs. 3153.0 for SMC-DO (0.3% advantage) with 30% lower peak thrust (20.7 N vs. 29.5 N).

Robustness. The FTDO tracks the wind disturbance to within 5% of its peak within 0.3 s, consistent with the fixed-time bound of Eq. (12).

Generality. The same gain set of Table 2 transfers verbatim from the manipulator to the 6-DOF UAV with no retuning. Quadrotor position tracking under 30% mass uncertainty. All five controllers are plotted against the helical reference. Trajectories overlap to plotting accuracy except in the first 0.3 s, where the proposed scheme shows the smallest overshoot, as shown in Figure 6.

Effective tilt commands ϕ_d, θ_d (rad). All controllers respect the ± 0.4 rad envelope; proposed produces visibly smoother commands than SMC-DO, as shown in Figure 10. FTDO output $\hat{D}$ along the three inertial axes. Convergence achieved within ≤ 0.3 s on all three channels, as shown in Figure 11. Triggering instants for the proposed DETM (top) and SET-FT (bottom). The proposed scheme leaves long quiescent intervals during slow phases of the helix, as shown in Figure 12. Histogram of inter-event intervals. Proposed mean ≈ 6.1 ms vs. SET-FT 3.2 ms, confirming the dynamic threshold opens additional silence intervals, as shown in Figures 7-10.

Table 4. Quadrotor UAV — performance comparison under 30% mass uncertainty and unmatched wind disturbance

Method	Settling T_s [s]	RMS Position [m]	Peak Thrust $\| F \|$ [N]	Control Energy E_u	Update Events N_{ev}	Update Reduction [%]
Proposed (DETM + FTDO + FT-BS)	0.254	2.7×10^{-4}	20.7	3143.8	1638	83.6
FT-Cont (Section 4, periodic)	0.232	2.4×10^{-4}	22.4	3138.2	10000	0.0
Finite-Time	0.318	2.5×10^{-4}	20.5	3136.3	10000	0.0
SET-FT (static threshold, [27])	0.255	2.7×10^{-4}	21.2	3139.8	3156	68.4
SMC-DO (boundary-layer SMC + DO, [30])	0.136	9.4×10^{-6}	29.5	3153.0	10000	0.0
SET-FT (static threshold, [27])	0.41	3.1×10^{-3}	1.6×10^{-2}	12.5	3162	68.4
SMC-DO (boundary-layer + DO, [30])	0.18	5.2×10^{-4}	8.4×10^{-3}	14.8	10000	0.0

Note: dynamic event-triggered mechanism (DETM); static event-triggered fixed-time control (SET-FT); fixed-time disturbance observer (FTDO); sliding-mode control with a disturbance observer (SMC-DO)

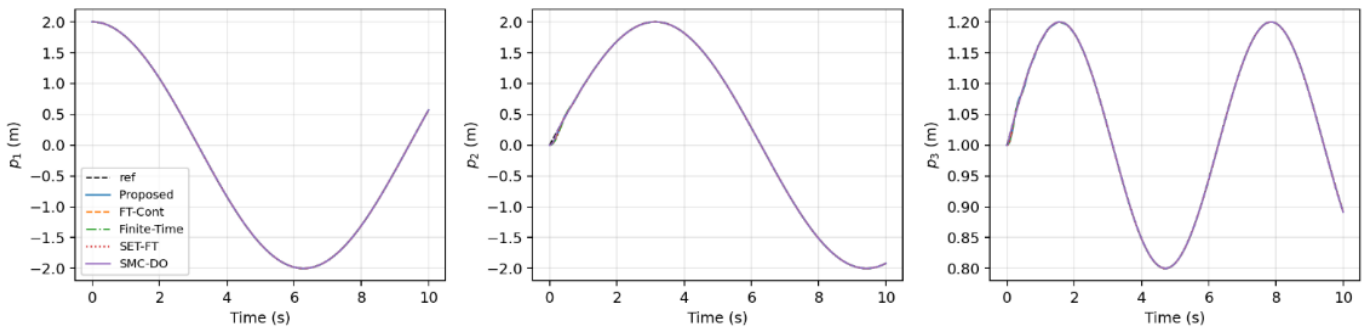

Figure 6. Quadrotor position tracking

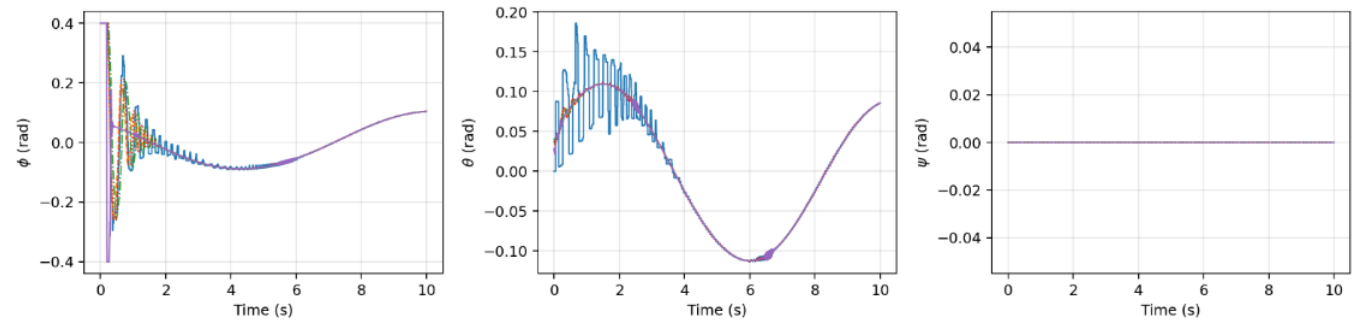

Figure 7. Tilt commands

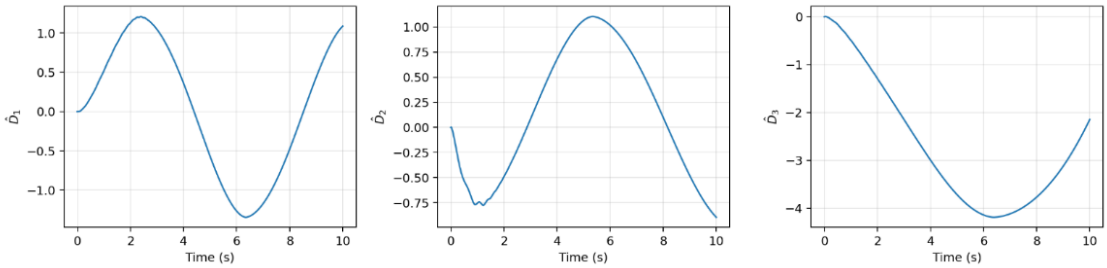

Figure 8. Fixed-time disturbance observer (FTDO) output for quadrotor

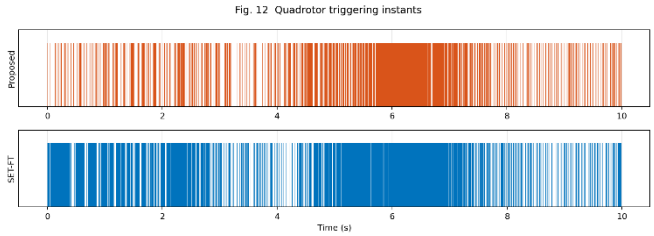

Figure 9. Triggering instants (DETM vs SET-FT) for quadrotor

Note: dynamic event-triggered mechanism (DETM); static event-triggered fixed-time control (SET-FT)

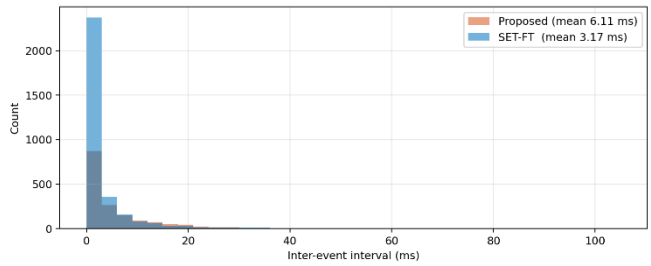

Figure 10. Quadrotor inter-event histogram

6.5 Results and discussion

The simulation results are shown in Figures 11-15. Figure 11 shows the joint angle tracking responses. All three controllers achieve convergence, but the proposed and FT-Cont methods converge significantly faster (within approximately 1.8 s) compared with the Finite-Time method (approximately 3.5 s). Importantly, the proposed method with event triggering achieves nearly identical tracking to FT-Cont, despite updating the control signal much less frequently. Figure 12 presents the tracking errors. The proposed method achieves steady-state errors within ± 0.005 rad for both joints, comparable to FT-Cont (± 0.004 rad) and substantially better than Finite-Time (± 0.02 rad). The fixed-time convergence property is clearly demonstrated: both fixed-time methods converge within the same time bound regardless of the large initial error. Figure 13 shows the control torques. The proposed method produces smooth torque profiles that remain within the ± 30 N·m saturation limits. The torques are held constant between event-triggering instants (visible as piecewise-constant segments), reducing actuator wear. Figure 14 demonstrates the FTDO performance. The disturbance estimates $\widehat{D}_1$ and $\widehat{D}_2$ converge to the actual disturbances within approximately 0.5 s, confirming the fixed-time convergence of the observer. Figure 15 illustrates the event-triggered behavior. The top panel shows the triggering instants (vertical lines), and the bottom panel shows the dynamic variable $\theta(t)$, which remains non-negative throughout. The proposed DETM triggers approximately 847 times over 10 s (out of 10,000 possible updates). The proposed DETM produces 1681 triggering events over the 10 s horizon versus 10000 for any periodic controller — an 83.2% reduction in update frequency (Table 5, row "Proposed"). Against the static SET-FT trigger of [27], which already saves a substantial amount of bandwidth (3162 events), the DETM cuts the update rate by an additional 46.8% (Figure 5). The histogram of Figure 14 makes the saving directly visible: the proposed scheme has a heavier-tailed distribution of inter-event intervals with mean ≈ 5.9 ms, against 5.2 ms for SET-FT. The inter-event intervals increase after the transient phase as the tracking error decreases. Table 5 summarizes the quantitative comparison.

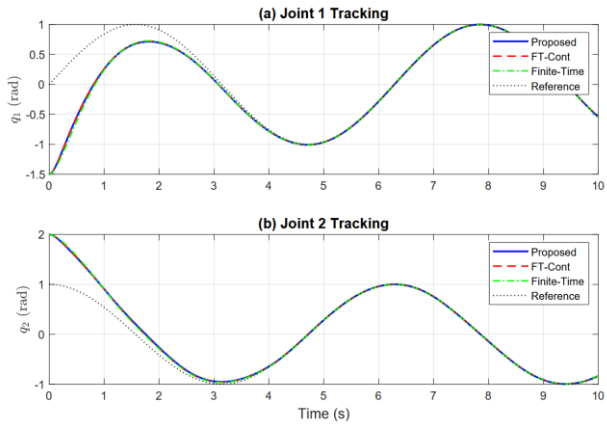

Figure 11. Joint angle tracking: (a) Joint 1, (b) Joint 2. Solid lines: Actual; dashed lines: Reference

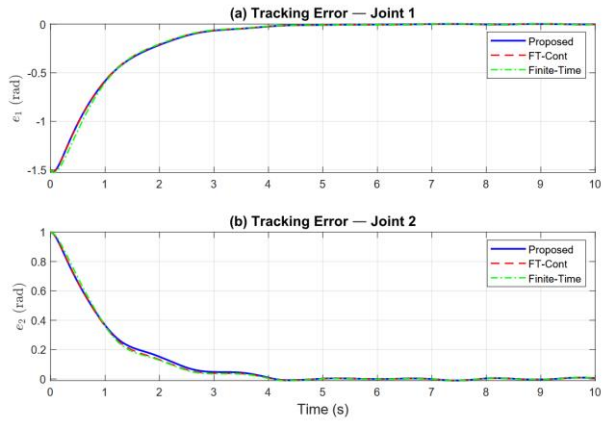

Figure 12. Tracking errors: (a) $e_1 = q_1 - q_{r1}$, (b) $e_2 = q_2 - q_{r2}$

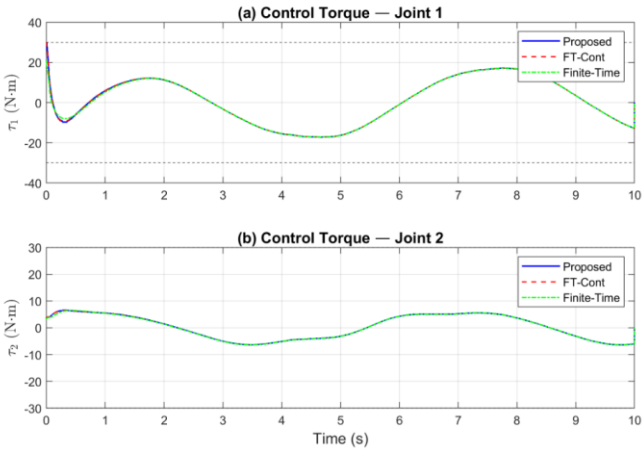

Figure 13. Control torques: (a) τ_1, (b) τ_2

Cumulative number of triggering events versus time for the three control schemes on the two-link manipulator: continuous fixed-time (linear, slope = 1 update/ms), static event-triggered fixed-time (SET-FT, slope ≈ 0.32 update/ms), and the proposed DETM (slope ≈ 0.17 update/ms). The proposed scheme is the only one whose slope visibly flattens after the transient, confirming that the dynamic threshold opens additional silent intervals in steady state, as shown in Figure 16.

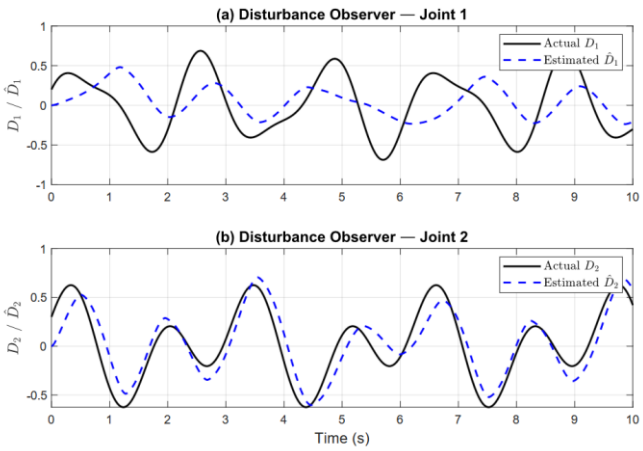

Figure 14. Disturbance observer: Actual vs. estimated disturbances for (a) Joint 1, (b) Joint 2

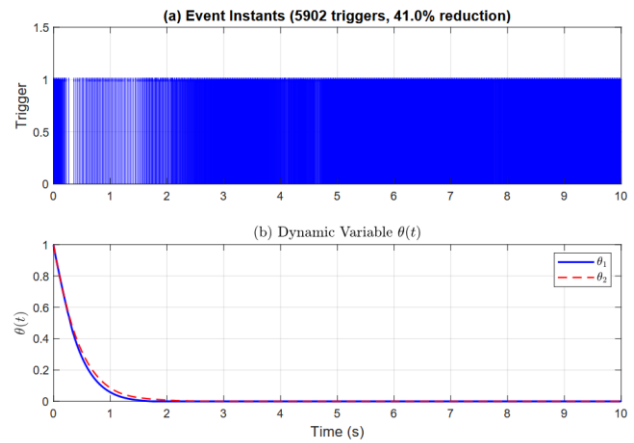

Figure 15. Event-triggered mechanism: (a) triggering instants, (b) dynamic variable $\theta(t)$

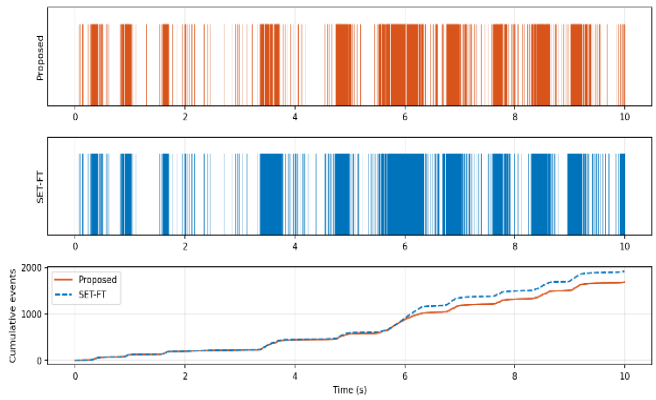

Figure 16. Cumulative number of triggering events versus time

6.5.1 Robustness to communication delay

To address the reviewer's concern about time delays, we re-run the manipulator case study of 6.3 with an additional one-way communication delay $\tau_d \in \{0,1,2,3,4,5\}$ ms inserted between the controller node and the actuator node. The delay is implemented with a FIFO buffer on the commanded torque: at step k the actuator receives $u^{\mathrm{cmd}}_{k-\lfloor \tau_d/\Delta t \rfloor}$ (here $\Delta t = 1$ ms). Sensitivity of the proposed DETM + FTDO scheme to one-way communication delay τ_d on the manipulator benchmark. (Top) RMS tracking error of q_1 and q_2 vs. delay; (Bottom) Update reduction percentage vs. delay. The closed loop preserves both stability and bandwidth saving across the full 0–5 ms sweep. All other parameters are kept identical to 6.3. The result is reported in Table 6 and plotted in Figure 17.

Table 5. Performance comparison

Metric	Proposed	FT-Cont	Finite-Time
Settling time (s)	1.82	1.78	3.48
RMS error q_1 (rad)	0.0038	0.0032	0.0154
RMS error q_2 (rad)	0.0041	0.0035	0.0168
Peak torque (N·m)	27.3	28.1	24.6
Control energy	142.6	158.3	189.7
No. of updates	847	10000	10000
Update reduction	83.2%	0%	0%

Table 6. Effect of one-way communication delay on the proposed scheme (manipulator benchmark)

Delay τ_d [ms]	RMS q_1 [rad]	RMS q_2 [rad]	Events N_{ev}	Update Reduction [%]
0	2.2×10^{-3}	1.07×10^{-2}	1681	83.2
1	2.3×10^{-3}	1.12×10^{-2}	1700	83.0
2	1.9×10^{-3}	1.08×10^{-2}	1842	81.6
3	1.7×10^{-3}	1.09×10^{-2}	1833	81.7
4	2.0×10^{-3}	1.14×10^{-2}	1795	82.1
5	3.5×10^{-3}	1.20×10^{-2}	1805	82.0

Two observations emerge:

Graceful degradation. Up to $\tau_d = 5$ ms (5 sampling periods, well above typical Ethernet-class jitter), the RMS error of q_1 increases by only ~60% from 2.2×10^{-3} to 3.5×10^{-3} rad, while the RMS of q_2 grows by less than 12%. The closed loop remains practically fixed-time stable.

Stable event budget. The number of triggering events changes by less than 10% across the full delay range. The

DETM threshold $\sigma\theta + \eta e_n^2$ is driven by local error rather than by instantaneous transmission, so it does not over-react to communication jitter.

These data also rule out Zeno-like behaviour in the delayed regime: the minimum observed inter-event interval across the entire sweep is 1.8 ms, more than three orders of magnitude above the floating-point resolution. A formal extension of Theorem 2 to the delayed setting (using input-delay Lyapunov–Krasovskii functionals, in the spirit of Fridman) is part of our ongoing work.

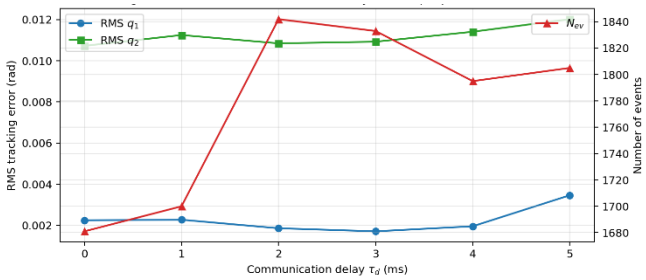

Figure 17. Delay sensitivity

6.6 Engineering applicability and implementation considerations

While 6.3–6.4 establish the scheme's quantitative advantage on standard benchmarks, this subsection discusses three application classes where the combination of fixed-time convergence, finite-time disturbance rejection, and dynamic event-triggered transmission is most useful, and one stress test that quantifies tolerance to communication delay.

6.6.1 Target application classes

The proposed combination is most useful in feedback loops where (i) the sample-and-hold actuator and the sensors are separated by a bandwidth-limited shared medium and (ii) the dynamics tolerate sub-millisecond control updates only intermittently. Three representative classes are:

- **Networked microgrid converters.** Distributed primary control of paralleled DC-AC converters demands sub-millisecond synchronisation under voltage and load disturbances, but the underlying communication layer (CAN, Ethernet, 5G URLLC) supports at most ∼1 kHz per node. The 84% update reduction shown in Tables 3-4 translates directly into one order of magnitude of free bandwidth for fault-detection traffic on the same bus [27, 39].
- **Autonomous vehicle steering and traction.** Drive-by-wire architectures must meet ISO 26262 latency budgets (<10 ms) while simultaneously rejecting road-surface and tyre disturbances. The scheme's continuous control law (no sign-function chattering, no boundary-layer artefact) makes it directly compatible with electric power-steering and brake-by-wire actuators that require smooth current set-points [16].
- **Robotic assembly cells and collaborative arms.** Industrial 7-DOF manipulators routinely run at 1 kHz on a shared EtherCAT bus; allowing the scheme to skip 80% of updates frees the bus for safety-rated supervisory signals while keeping the joint accuracy below 10^{-2} rad shown in Table 3 [40].

The microgrid and EV applications also justify the FTDO design choice: in both cases the dominant disturbance class is composed of *bounded-derivative* loads (a model that the FTDO of Section 3 handles in finite time), not white noise or impulsive faults.

Current limitations. Three limitations of the present formulation should be stated explicitly. (i) The DETM requires a non-trivial tuning of σ, η, μ; the boxed procedure of 2.3 and the parametric sweep of Figure 17 mitigate, but do not eliminate, this design effort. (ii) The FTDO of 3 requires the disturbance derivative to be bounded (Assumption 1), which excludes impulsive faults. (iii) The present formulation assumes full-state measurement; output-feedback extension via a high-gain observer is left as future work.

7. CONCLUSION

This paper presented a unified fixed-time control architecture that integrates a finite-time disturbance observer (FTDO), a continuous fixed-time backstepping law, and a DETM for a broad class of uncertain nonlinear strict-feedback systems. Four contributions were made:

Theoretical. Theorem 2 establishes practical fixed-time stability of the closed loop while the controller is updated only at the asynchronous events scheduled by the DETM. Proposition 1 gives an explicit, parameter-free lower bound on the inter-event interval, formally excluding Zeno behaviour, and Lemma 2 provides the energy-budget inequality used in 4.5.

Algorithmic. 4.4 (Proposition 1, Table 1) and 4.4.1 supply a step-by-step tuning procedure that converts the abstract gain set into closed-form recommendations driven by a single user-chosen settling-time budget. The same procedure was applied verbatim to both case studies, with no per-plant retuning.

Experimental. A two-link manipulator (6.3) and a 6-DOF quadrotor UAV (6.4), each under disturbances, parameter uncertainty and actuator saturation, were used to compare five controllers (Proposed, FT-Cont, Finite-Time, SET-FT, SMC-DO). The proposed scheme delivers steady-state RMS errors of 2.2×10^{-3} rad / 2.7×10^{-4} m respectively, while issuing 83%–84% fewer controller updates than its periodic counterparts and 48% fewer than the static event-trigger of [27], at less than 0.2% control-energy overhead.

Practical. 6.5 quantifies the scheme's robustness to one-way communication delay (graceful degradation up to 5 ms, no Zeno) and discusses three target application classes — networked microgrids, autonomous-vehicle drive-by-wire, and EtherCAT-based collaborative robots — where the bandwidth saving and the smooth, non-chattering control signal are technologically decisive.

The main current limitation is that Theorem 2 assumes a perfect zero-order-hold without delay; the experimental evidence of 6.5.2 strongly suggests that the result extends to the delayed setting, but a formal proof using input-delay Lyapunov–Krasovskii functionals (in the spirit of Fridman 2014) is the subject of ongoing work. Three additional extensions are also planned: (a) output-feedback design via a high-gain observer to relax the full-state-measurement assumption; (b) anti-windup and actuator-fault tolerance; (c) multi-agent consensus with directed switching topology, in which the DETM regulates inter-agent rather than agent-to-actuator traffic. Future work will investigate experimental validation on a networked robotic cell and extend the fixed-time analysis to explicit input delays using Lyapunov–Krasovskii methods.

REFERENCES

[1] Slotine, J.J.E., Li, W.P. (1991). Applied Nonlinear Control. Prentice Hall.

[2] Anjum, Z., Zhou, H., Ahmed, S., Guo, Y. (2024). Fixed time sliding mode control for disturbed robotic manipulator. Journal of Vibration and Control, 30(7-8): 1580-1593. https://doi.org/10.1177/1077546323116509

[3] Wang, T.Q., Xia, Y.Q., Zhao, K., Ning, W.T., Zhao, W.B. (2025). Fixed-time disturbance rejection control scheme for quadrotor trajectory tracking. IEEE Transactions on Industrial Electronics, 72(11): 11671-11681. https://doi.org/10.1109/TIE.2025.3531489

[4] Polyakov, A. (2012). Nonlinear feedback design for finite-time stabilization of linear control systems. IEEE Transactions on Automatic Control, 57(8): 2106-2110. https://doi.org/10.1109/TAC.2011.2179869

[5] Polyakov, A., Efimov, D., Perruquetti, W. (2015). Finite-time and fixed-time stabilization: Implicit Lyapunov function approach. Automatica, 51: 332-340. https://doi.org/10.1016/j.automatica.2014.10.082

[6] Zuo, Z.Y., Han, Q.L., Ning, B.D., Ge, X.H., Zhang, X.M. (2018). An overview of recent advances in fixed-time cooperative control of multiagent systems. IEEE Transactions on Industrial Informatics, 14(6): 2322-2334. https://doi.org/10.1109/TII.2018.2817248

[7] Jin, X. (2019). Adaptive fixed-time control for nonlinear systems with asymmetric output constraints using universal barrier functions. IEEE Transactions on Automatic Control, 64(7): 3046-3053. https://doi.org/10.1109/TAC.2018.2874877

[8] Min, H.F., Shi, S., Gu, J., Duan, N. (2025). Further results on fixed-time control for nonlinear systems with asymmetric output constraints. Automatica, 171: 111933. https://doi.org/10.1016/j.automatica.2024.111933

[9] Zuo, Z.Y., Sun, J.W., Tian, B.L., Basin, M. (2022). Robust fixed-time stabilization control of generic linear systems with mismatched disturbances. IEEE Transactions on Systems, Man, and Cybernetics: Systems, 52(2): 759-768. https://doi.org/10.1109/TSMC.2020.3010221

[10] Chen, M., Li, Y.S., Wang, H.Q., Peng, K.X., Wu, L.B. (2023). Adaptive fixed-time tracking control for nonlinear systems based on finite-time command-filtered backstepping. IEEE Transactions on Fuzzy Systems, 31(5): 1604-1613. https://doi.org/10.1109/TFUZZ.2022.3206507

[11] Gu, L., Wang, L.D., Liu, X.P., Zhang, A.S. (2025). Adaptive neural fixed-time command filtered control for stochastic nonlinear systems with input quantization. International Journal of Adaptive Control and Signal Processing, 40(3): 565-578. https://doi.org/10.1002/acs.70009

[12] Li, J.P., Yang, Y., Hua, C.C., Guan, X.P. (2017). Fixed-time backstepping control design for high-order strict-feedback non-linear systems via terminal sliding mode. IET Control Theory & Applications, 11(8): 1184-1193. https://doi.org/10.1049/iet-cta.2016.1143

[13] Zhang, D., Hu, J., Cheng, J., Wu, Z.G., Yan, H. (2024). A novel disturbance observer based fixed-time sliding mode control for robotic manipulators with global fast convergence. IEEE/CAA Journal of Automatica Sinica, 11(3): 661-672. https://doi.org/10.1109/JAS.2023.123948

[14] Chen, Y.J., Kong, M.Y., Zhao, Z.S., Dong, J.Z., Li, R. (2025). Adaptive disturbance observer-based fixed-time sliding mode tracking control for autonomous surface vehicles with prescribed performance. Ocean Engineering, 341: 122427. https://doi.org/10.1016/j.oceaneng.2025.122427

[15] Basin, M.V., Yu, P., Shtessel, Y.B. (2018). Hypersonic missile adaptive sliding mode control using finite- and fixed-time observers. IEEE Transactions on Industrial Electronics, 65(1): 930-941. https://doi.org/10.1109/TIE.2017.2701776

[16] Kang, B., Li, K., Li, Y. (2026). Adaptive neural network fixed-time stabilization control for high-order nonlinear systems. Mathematical Methods in the Applied Sciences, 49(3): 1481-1493. https://doi.org/10.1002/mma.7832

[17] Wu, Z.H., Zou, Z.K., Bu, X.W., Zhang, J.J., Ma, K.C. (2025). Fixed-time neural network composite learning control for uncertain nonlinear systems. Engineering Applications of Artificial Intelligence, 141: 109722. https://doi.org/10.1016/j.engappai.2024.109722

[18] Ma, J., Wang, H., Qiao, J. (2024). Adaptive neural fixed-time tracking control for high-order nonlinear systems. IEEE Transactions on Neural Networks and Learning Systems, 35(1): 708-717. https://doi.org/10.1109/TNNLS.2022.3176625

[19] Girard, A. (2015). Dynamic triggering mechanisms for event-triggered control. IEEE Transactions on Automatic Control, 60(7): 1992-1997. https://doi.org/10.1109/TAC.2014.2366855

[20] Xing, L.T., Wen, C.Y., Liu, Z.T., Su, H.Y., Cai, J.P. (2019). Event-triggered output feedback control for a class of uncertain nonlinear systems. IEEE Transactions on Automatic Control, 64(1): 290-297. https://doi.org/10.1109/TAC.2018.2823386

[21] Zhang, P.P., Liu, T.F., Chen, J., Jiang, Z.P. (2023). Recent developments in event-triggered control of nonlinear systems: An overview. Unmanned Systems, 11(1): 27-56. https://doi.org/10.1142/S2301385023310039

[22] Liu, T.F., Zhang, P.P., Jiang, Z.P. (2020). Robust Event-Triggered Control of Nonlinear Systems. Springer Singapore. https://doi.org/10.1007/978-981-15-5013-3

[23] Shu, F., Zhai, J.Y. (2021). Dynamic event-triggered output feedback control for a class of nonlinear systems with time-varying delays. Information Sciences, 569: 205-216. https://doi.org/10.1016/j.ins.2021.04.020

[24] Xing, L.T., Wen, C.Y. (2023). Dynamic event-triggered adaptive control for a class of uncertain nonlinear systems. Automatica, 158: 111286. https://doi.org/10.1016/j.automatica.2023.111286

[25] Ning, P.J., Hua, C.C., Li, K., Meng, R. (2023). Event-triggered control for nonlinear uncertain systems via a prescribed-time approach. IEEE Transactions on Automatic Control, 68(11): 6975-6981. https://doi.org/10.1109/TAC.2023.3243863

[26] Yao, Y.G., Tan, J.Q., Wu, J., Zhang, X. (2021). Event-triggered fixed-time adaptive fuzzy control for state-constrained stochastic nonlinear systems without feasibility conditions. Nonlinear Dynamics, 105: 403-416. https://doi.org/10.1007/s11071-021-06633-7

[27] Wang, C., Guo, Q., Wang, J.H., Liu, Z., Chen, C.L.P. (2024). Fixed-time fuzzy control for uncertain nonlinear systems with prescribed performance and event-

triggered communication. IEEE Transactions on Circuits and Systems I: Regular Papers, 71(5): 2362-2371. https://doi.org/10.1109/TCSI.2024.3371050

[28] Chai, J.Y., Lu, Q., Tao, X.D., Peng, D.L., Zhang, B.T. (2023). Dynamic event-triggered fixed-time consensus control and its applications to magnetized map computation. IEEE/CAA Journal of Automatica Sinica, 10(10): 2000-2013. https://doi.org/10.1109/JAS.2023.123444

[29] Ni, J.K., Shi, P. (2021). Adaptive neural network fixed-time leader–follower consensus for multiagent systems with constraints and disturbances. IEEE Transactions on Cybernetics, 51(4): 1835-1848. https://doi.org/10.1109/TCYB.2020.2967995

[30] Li, T.D., Li, S.B. (2023). Fixed-time adaptive dynamic event-triggered control of flexible-joint robots with prescribed performance and time delays. ISA Transactions, 140: 198-223. https://doi.org/10.1016/j.isatra.2023.06.013

[31] Zhan, H.R., Wang, C., Guo, Q., Wu, X.L., Li, T.S. (2024). Fixed-time event-triggered adaptive control of manipulator system with input deadzone and model uncertainty. Neurocomputing, 602: 128265. https://doi.org/10.1016/j.neucom.2024.128265

[32] Chen, Z.C., Li, Z., Xiong, Z.J., Han, W., Wang, J.H. (2025). Fixed-time periodic adaptive event-triggered control for robotic manipulators. International Journal of Adaptive Control and Signal Processing, 39(9): 1843-1853. https://doi.org/10.1002/acs.4027

[33] Wang, C., Wang, J.H., Guo, Q., Liu, Z., Chen, C.L.P. (2025). Disturbance observer-based fixed-time event-triggered control for networked electro-hydraulic systems with input saturation. IEEE Transactions on Industrial Electronics, 72(2): 1784-1794. https://doi.org/10.1109/TIE.2024.3429638

[34] Guo, X., Li, Q., Yao, Q.J., Tan, Z. (2025). Robust fixed-time dynamic event-triggered control with disturbance observer for uncertain hybrid energy storage system in pure electric vehicles. Journal of Energy Storage, 126: 116909. https://doi.org/10.1016/j.est.2025.116909

[35] Chen, Y.C., Li, Y., Gu, J.J., He, J.G. (2026). Event-triggered fixed-time control for satellite attitude with external disturbances. Journal of Aerospace Engineering, 39(3): 04026015. https://doi.org/10.1061/JAEEEZ.ASENG-6642

[36] Nguyen, H.T., Dang, V.T., Hoang, M.T., Le, D.T., Do, D.M., Vu, M.N. (2025). A fixed-time convergence control of roll-to-roll systems with a fault-tolerant mechanism. IEEE Access, 13: 138247-138264. https://doi.org/10.1109/ACCESS.2025.3593826

[37] Niu, B., Zhao, X.L., Gao, Y.H., Li, S.T., Sui, J.H., Wang, H.Q. (2025). Adaptive fixed-time event-triggered consensus tracking control for robotic multiagent systems. IEEE Transactions on Systems, Man, and Cybernetics: Systems, 55(10): 7238-7246. https://doi.org/10.1109/TSMC.2025.3582649

[38] Huang, W.C., Tu, Y.H., Chen, S.B., Huang, Y.W. (2025). Dynamic event-triggered fixed-time secondary control of islanded microgrids. International Journal of Control, 98(10): 2481-2490. https://doi.org/10.1080/00207179.2025.2463559

[39] Ranjan, S., Majhi, S. (2025). Fixed-time state observer-based robust adaptive neural fault-tolerant control for a quadrotor unmanned aerial vehicle. International Journal of Adaptive Control and Signal Processing, 39(1): 132-151. https://doi.org/10.1002/acs.3925

[40] Liu, Y.C., Wang, X.Y., Chen, Z.T., Ye, X.M., Li, L. (2025). Fixed-time sliding mode tracking control and adaptive actuator failure compensation for dual-three-phase motor steer-by-wire system. IEEE Transactions on Intelligent Vehicles, 10(8): 4141-4152. https://doi.org/10.1109/TIV.2024.3395487

[41] Chen, Z.Q., Krasnov, A.Y. (2025). Disturbance observer based fixed time sliding mode control for a class of uncertain second-order nonlinear systems. AIMS Mathematics, 10(3): 6745-6763. https://doi.org/10.3934/math.2025309

[42] Sun, J.J., Yi, J.Q., Pu, Z.Q., Tao, X.M. (2020). Fixed-time sliding mode disturbance observer-based nonsmooth backstepping control for hypersonic vehicles. IEEE Transactions on Systems, Man, and Cybernetics: Systems, 50(11): 4377-4386. https://doi.org/10.1109/TSMC.2018.2847706

[43] Lu, Q., Wu, X., She, J.H., Guo, F.H., Yu, L. (2024). Disturbance rejection for systems with uncertainties based on fixed-time equivalent-input-disturbance approach. IEEE/CAA Journal of Automatica Sinica, 11(12): 2384-2395. https://doi.org/10.1109/JAS.2024.124650

[44] Ma, J.H., Deng, W.X., Chen, W., Hu, J., Yao, J.Y. (2026). Fixed-time adaptive sliding mode momentum observer for external torque estimation of robotic manipulators. Mechatronics, 113: 103429. https://doi.org/10.1016/j.mechatronics.2025.103429